DFT-based adsorption isotherms for pure and flue gas mixtures including SO_2 poisoning on Mg-MOF-74

Gerard Alonso,[‡] Daniel Bahamon,[‡] Fatemeh Keshavarz,[§] Xavier Giménez,[‡] Pablo Gamallo[‡] and Ramón Sayós[‡*]

[‡] Departament de Ciència de Materials i Química Física & Institut de Química Teòrica i Computacional (IQTCUB), Universitat de Barcelona, C. Martí i Franquès 1, 08028 Barcelona, Spain.

[§] Department of Chemistry, College of Sciences, Shiraz University, 71454, Shiraz, Iran.

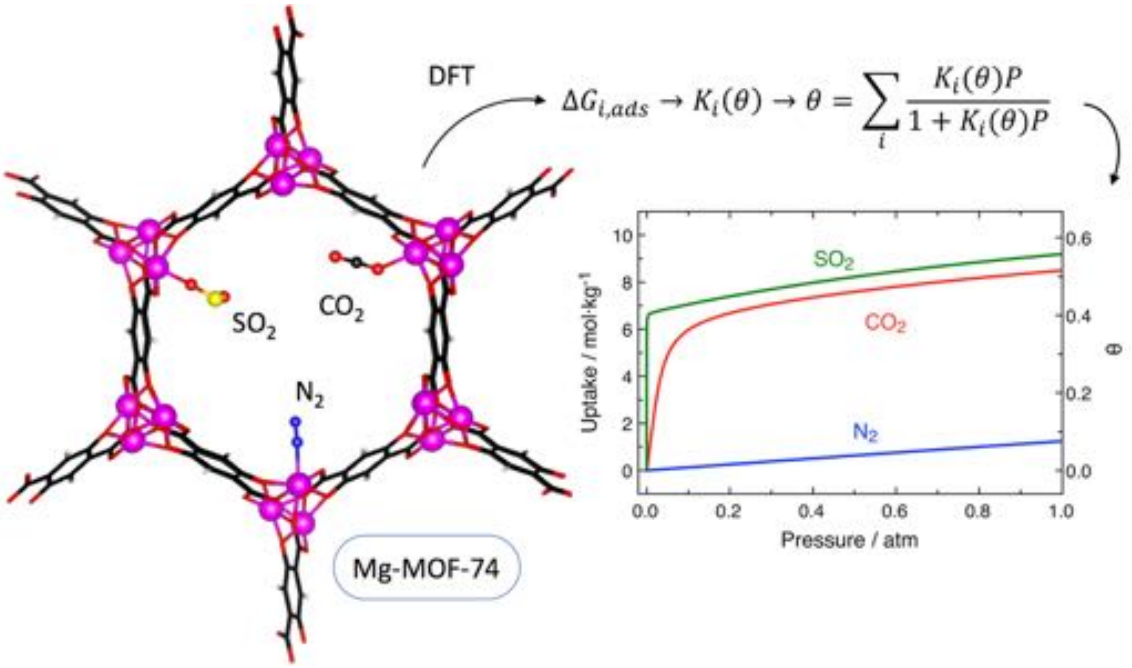

(graphical abstract)

ABSTRACT

A simplified model is applied for the prediction of gas/solid adsorption isotherms of pure gases (i.e., CO_2, N_2, SO_2) on the metal-organic framework Mg-MOF-74, based on periodic Density Functional Theory (DFT) calculations and a dual-site Langmuir approach (DFT/DSL), using a mean-field approximation for the inclusion of the lateral interactions. This model not only provides reliable adsorption isotherms ($P \leq 1$ atm, $293 \leq T \leq 373$ K) but also isosteric heats of adsorption in good agreement with both available experimental data and previous more refined models. Moreover, an extension of this model is used to study the effect of SO_2 as an impurity in the efficiency of adsorption and desorption processes of some post-combustion gas mixtures. It is shown that a very low concentration of SO_2 is enough to poison Mg-MOF-74 structure. Moreover, different swing adsorption techniques at different working conditions are analysed to reduce the impact of SO_2 poisoning in CO_2 separation.

Manuscript submitted to The Journal of Physical Chemistry A (Jan 26th, 2018)

1. INTRODUCTION

Over the past decades, many efforts have been addressed for Carbon Capture, Utilization and Storage (CCUS) technologies on flue gas streams.[1,2] Several post-combustion CO_2 capture technologies including absorption, adsorption, cryogenics, membranes and so forth, have been studied.[3] Nowadays, most separation technologies involve solvents (e.g., amines), which demand high energy and result in potential unwanted environmental and economic consequences due to solvent loss and degradation.[4]

Alternative technologies aimed to mitigate some of the disadvantages of these amine solutions have become an active area of research. Among them, solid absorbent materials have demonstrated potential capability in reducing costs and improving CCUS performance compared to existing systems.[5,6] Finding the most efficient absorbents has attracted a lot of both experimental and theoretical research, and even a wide variety of new absorbents have been proposed and synthesized for using in post-combustion CO_2 capture.[7,8,9,10,11,12,13]

Metal−Organic Frameworks (MOFs) have received significant attention. They are porous structures, with high thermal stability,[14] adjustable chemical functionality,[15] extra-

high porosity,[16] and hundreds of crystalline well-characterized porous structures are available [17,18,19,20,21]. In fact, some of them have demonstrated high CO_2 adsorption capacities and high selectivities for CO_2 over N_2, in addition to reduced regeneration energy penalties. [5,22,23,24,25] One of the most interesting MOF for CO_2 capture is Mg-MOF-74 (also known as CPO-27-Mg or Mg_2(DOBDC)).[26] This MOF is based on helical chains of Mg^{2+} located at the intersections of honeycomb-like structures formed by 2,5-dioxido-1,4-benzenedicarboxylate ($DOBDC^{4-}$) [27] linkers with large one-dimensional pores of approximately 12 Å diameter. Mg^{2+} atoms present an octahedral coordination with oxygen atoms of linkers. Each Mg^{2+} ion in the evacuated structure bears an open-metal site, which is a highly favourable adsorption site for various guest molecules. Currently, Mg-MOF-74 displays one of the best adsorption performances for many gas molecules, with CO_2 uptakes as high as 8.08 mol·kg^{-1} at 298 K and 1.0 atm, associated with a high initial isosteric heat of adsorption value (i.e., 47 kJ/mol at low surface coverages).[27] The unsaturated sites are the cause of strong interactions with CO_2 molecules due to its large quadrupole moment and polarizability.[28]

Nevertheless, in general, it has been shown that the presence of gas impurities in the flue gas mixture affects the efficiency of carbon dioxide capture processes.[29,30,31] Although there are noticeable studies on adsorption of CO_2 and some other gases on Mg-MOF-74, limited studies have concerned the effect of impurities such as SO_2 and NO_x on the CO_2 capture process on MOFs.[32,33,34,35]

In this regard, molecular simulation methods, such as Grand Canonical Monte Carlo and Molecular Dynamics have made an important contribution to the understanding of gas adsorption and separation in porous materials.[36] In general, these studies use suitable force fields for predicting the intermolecular solid/fluid and fluid/fluid interactions, which are less expensive than quantum-chemical calculations [37,38,39] for the evaluation of energies and forces.

Recent theoretical studies on Mg-MOF-74 [40,41] revealed that the correct description of gas/MOF dispersion corrected DFT adsorption energies, partition functions and gas/gas lateral interactions, which can be used to obtain thermodynamic functions at different coverages (i.e., $\Delta U(\theta)_{ads}, \Delta H(\theta)_{ads}, \Delta S(\theta)_{ads}$ and $\Delta G(\theta)_{ads}$), can be combined in a multi-site Langmuir model to predict adsorption isotherms at any temperature and pressure. These electronic structure calculations are able to reproduce the gas/metal interactions accurately, that will be the main driving force of adsorption at

low pressures, and also the gas/gas interactions, which can have an important effect in the adsorption properties of Mg-MOF-74 at high pressures. Additionally, the reliable gas/MOF interactions described by DFT ensures the correct evaluation of poisoning effects at low concentration of pollutants (i.e., < 1 mol %), which is controlled by the competition for MOF sites between the pollutants and other gas molecules.

Among the works previously published, Sillar et al. recently studied the adsorption of CO_2 in Mg-MOF-74 using a dual-site Langmuir model enhanced with gas/gas lateral interactions. Their adsorption energies and other thermodynamic functions were calculated using a combination of periodic and high accuracy cluster models; for more information, the reader is referred to the original paper. [40] Also, they obtained the lateral interactions with the calculation of each pair of interacting molecules explicitly and then, the coverage dependent lateral interactions were averaged to be treated as a mean-field. The present work intends to simplify the model of Sillar et al. by using only periodic DFT calculations instead of a combination of periodic and cluster models, and also reducing the number of calculations needed to build a reasonable adsorption isotherm to only four adsorption processes, which is possible by simplifying the model of the gas/gas lateral interactions. With the previous simplifications in the model of Sillar et al., pure adsorption isotherms and the coverage dependent differential isosteric heats were predicted for CO_2, N_2 and SO_2 in good comparison with both the previous theoretical and experimental results when available. Furthermore, combination of DFT calculations with dual-site Langmuir model (DFT/DSL) was extended to treat ternary mixtures of CO_2, N_2 and SO_2 with the aim of quantifying the SO_2 poisoning impact on a model flue gas stream.

2. METHODS AND COMPUTATIONAL DETAILS

2.1 Density Functional Theory Calculations. The adsorption of gas molecules onto Mg-MOF-74 was first studied by means of periodic DFT calculations performed with Vienna *ab-initio* Simulation Package (VASP).[42,43] The dispersion corrected VDW-DF2 functional [44,45] was selected because it accurately reproduces gas/MOF interactions, especially the CO_2/MOF binding energies accounting also for van der Waals interactions.[46] The projected augmented wave potential [47] (PAW) technique was used for the core electrons, while valence electrons were treated explicitly with a plane wave expansion with a kinetic energy cut-off of 600 eV. All calculations were carried out with a reciprocal cell containing only the Γ point due to the large size of the real simulation cell, and interaction energies and forces were converged up to 10^{-6} eV and 10^{-4} eV/Å, respectively.

The simulation cell used is the rhombohedral structure presented in Figure 1, which contains 12 Mg^{2+} sites and 12 ($DOBDC^{4-}$) Linker sites per pore, and it is large enough in all directions to prevent the interactions of the adsorbed gas molecules with their periodic images. Gas/MOF adsorption energies (ΔE_{ads}) were calculated according to eq 1, first minimizing the full MOF structure at VDW-DF2 level, and then relaxing the gas molecule on the surface along with the nearest MOF atoms (i.e., those surface atoms closer than 7 Å to any atom of the gas molecule). All minima were characterized with frequency calculations that were used to obtain the corresponding partition functions [48] necessary to calculate the adsorption thermodynamic functions ΔH_{ads} and ΔS_{ads}, which can be related to ΔG_{ads} through eq 2. In our model, translational, rotational and vibrational partition functions were calculated for the gas molecules, but 3N normal modes were considered as harmonic vibrations after adsorption (i.e., all pure vibrational modes along with the frustrated rotations and translations). The translations, rotations and vibrations of the substrate were neglected because they remained almost constant upon gas adsorption, and its contribution vanished when ΔG_{ads} was calculated. To ensure the validity of this approximation, the adsorption of one CO_2 molecule onto a Mg^{2+} site at 298 K was calculated considering the vibrations of the 61 nearest MOF atoms resulting in a negligible difference in the final ΔG_{ads} value (i.e., 1.05 kJ/mol). For more detailed

information on the present calculation of all thermodynamic functions obtained from DFT data the reader is referred to Sect. S1 of the Supporting Information).

$$\Delta E_{ads} = E_{MOF/gas} - E_{MOF} - E_{gas} \quad (1)$$

$$\Delta G_{ads} = \Delta H_{ads} - T\Delta S_{ads} \quad (2)$$

2.2 Obtaining Isotherms from a DFT-based Dual-Site Langmuir Adsorption Model. To predict the adsorption isotherm of a pure gas onto a surface, the single-site Langmuir isotherm model cannot be successfully used due to the assumptions made by Langmuir in its derivation [49] : i) all sites are equivalent, ii) there are no interactions between molecules, and iii) each site can hold at most one molecule. The first assumption does not apply in our case because Mg-MOF-74 presents two main different adsorption sites.[26] The second assumption neglects adsorbate lateral interactions, which may have important effects as shown in the discussion of this work and by other authors.[40,41,50] Finally, the third statement in principle will be true at low pressures for small gas species according to previous experimental and theoretical adsorption studies on MOFs. [35,46,51,52] For these reasons, two different adsorption sites are accounted for by using a dual-site Langmuir isotherm model (eq 3),[53] which assumes that the coverage at each adsorption site is governed by a single Langmuir isotherm with its own equilibrium constant. With this assumption, the total coverage *(θ)* can be obtained by the sum of two individual Langmuir isotherms, the first regarding the coverage of Mg^{2+} sites *(θ_{Mg2+})* and the second accounting for the coverage at the Linker sites *(θ_L)*, multiplied by the site distribution $\chi_i = N_i/N_{tot}$, with *i* = Mg^{2+} or *L*, and N_{tot} the total number of sites. In Mg-MOF-74 the number of Mg^{2+} and Linker sites is the same, which implies that $\chi_{Mg2+} = \chi_L = 0.5$. On the other hand, the gas-gas lateral interactions will modify the adsorption Gibbs free energy with the surface coverage, which makes the equilibrium constant to be also dependent on this magnitude (eq 4) [53],

$$\theta = \chi_{Mg2+}\theta_{Mg2+} + \chi_L\theta_L = \chi_{Mg}\frac{K_{Mg2+}(\theta)\,P}{1+K_{Mg2+}(\theta)\,P} + \chi_L\frac{K_L(\theta)\,P}{1+K_L(\theta)\,P} \quad (3)$$

$$K_i(\theta) = \frac{1}{P_o}e^{-\Delta G_{i,ads}(\theta)/RT} \quad (4)$$

being P_o the standard pressure (i.e., 1 atm).

With eqs 3-4 one can obtain the adsorption isotherm of a pure gas species adsorbed on the Mg-MOF-74 surface from $\boldsymbol{\Delta G_{i,ads}(\theta)}$ for both Mg^{2+} and Linker sites, which formally depends on the temperature and the surface coverage of both sites. In this work, we simplified the calculation of lateral interactions assuming that $\boldsymbol{\theta_L}$ is small according to previous theoretical and experimental adsorption studies with many gases at the selected pressures of the present work [26,51,54]. This assumption implies that $\boldsymbol{\Delta G_{i,ads}(\theta)}$ in our model will only depend on the temperature, the nature of the adsorption site (*i*) and the coverage on Mg^{2+} sites ($\boldsymbol{\theta_{Mg2+}}$). A mean-field (MF) approximation is used [55,56] to evaluate the coverage dependence in $\boldsymbol{\Delta G_{i,ads}(\theta)}$, which is considered a linear function between $\boldsymbol{\Delta G_{i,ads}(\theta \approx 0)}$, when adsorbing a gas molecule in the empty framework, and $\boldsymbol{\Delta G_{i,ads}}$, when adsorbing a molecule in a Mg^{2+} fully loaded structure, both values calculated with eq 2. Within this approximation $\boldsymbol{\Delta\left(\Delta G_{i,ads}\right)}$ is defined as the difference between the Mg^{2+} full-coverage and the zero-coverage values, being the final coverage dependent Gibbs free energy defined by eq 5.

$$\Delta \boldsymbol{G_{i,ads}(\theta) = \Delta G_{i,ads}(\theta \approx 0) + \theta_{Mg2+} \cdot \Delta(\Delta G_{i,ads})} \quad (5)$$

In order to obtain the coverage at equilibrium at a given pressure *(P)* and temperature *(T)* using $\boldsymbol{\Delta G_{i,ads}}$ DFT values, eq 3-5 must be solved iteratively by using $\boldsymbol{\Delta G_{i,ads}(\theta \approx 0)}$ quantity as initial value in the first iteration and replacing the result of $\boldsymbol{\theta_{Mg2+}}$ obtained from eq 3 into eq 5 until the convergence of the total coverage ($\boldsymbol{\theta}$) is achieved. Although this method allows obtaining adsorption isotherms by only characterizing the adsorption sites and its lateral interactions, the final adsorption isotherms obtained by this method will be reliable at moderate pressures and temperatures. Also, the mean-field approximation considers the effect of co-adsorption as an average field, instead of a local effect. This implies that molecular arrangements such as islands cannot be observed with this method. However, the present work demonstrates that even with these limitations, this DFT/DSL model can successfully predict adsorption isotherms and isosteric heats of adsorption with a high degree of accuracy.

2.3 Prediction of the Isosteric Heat Dependence with Coverage in Mg-MOF-74. The adsorption enthalpy (integral value) can be obtained by summing the enthalpy of adsorption contributions of both sites (eq 6),

$$\Delta H_{ads}(\theta) = \theta_{Mg2+} \cdot \Delta H_{Mg2+,ads}(\theta) + \theta_L \cdot \Delta H_{L,ads}(\theta) \quad (6)$$

where each enthalpy depends on the temperature, the nature of the adsorption site and the surface coverage, so mean-field approximation is also applied to determine the value of $\Delta H_{i,ads}(\theta)$ with an expression analogous to eq 5 but using enthalpies instead of Gibbs free energies.

The isosteric heat of adsorption (q_{st}) can be obtained from the partial derivative of $\Delta H_{ads}(\theta)$ with respect to the coverage at constant temperature (eq 7).[57,58]

$$q_{st} = -\left(\frac{\partial \Delta H_{ads}}{\partial \theta}\right)_T \quad (7)$$

Alternatively, q_{st} was also calculated using the Clausius-Clapeyron equation,[59] which arises from the slope of the ln(P) vs. 1/T isostere (eq 8). This methodology is extensively used in experimental studies and requires the measurement or calculation of isotherms at different temperatures to build the isostere, assuming that ΔH_{ads} is approximately constant in the working range of temperatures. Both methods were used and compared to obtain q_{st} at several coverages and temperatures, showing equivalent results.

$$\left(\frac{\partial \ln(P)}{\partial(\frac{1}{T})}\right)_\theta = \frac{q_{st}}{R} \quad (8)$$

3. RESULTS AND DISCUSSION

3.1 Analysis of the Main Adsorption Sites: DFT Adsorption Energies, Enthalpies, Entropies and Gibbs Free Energies. The adsorption of single CO_2, N_2 and SO_2 molecules onto the two main adsorption sites (taken here as approximately zero-

coverage) was analysed at DFT level, showing in all cases that Mg^{2+} is the most favourable site when compared to the Linker. These sites are shown in Figure 2 with CO_2 molecules adsorbed on them. The adsorption energies obtained (including ZPE) onto the Mg^{2+} sites were -46.1 kJ/mol, -29.3 kJ/mol and -78.9 kJ/mol for CO_2, N_2 and SO_2, respectively, in good agreement with the theoretical results available in the bibliography (i.e., -41.0/-44.9 kJ/mol for CO_2,[60,61,62,63] -28.0/-28.5 kJ/mol for N_2 [62,63] and -62.0/-88.0 kJ/mol for SO_2 [62,63,64]). Also, these results show a much stronger adsorption for SO_2 than for CO_2 according to the poisonous nature of SO_2 [29]. In contrast, the adsorption on the Linker sites presents a binding energy of -29.5 kJ/mol for CO_2 and -36.6 kJ/mol for SO_2, while no adsorption is observed for N_2. Unfortunately, to our knowledge, there are no data reported on the adsorption properties of the Linker for these molecules, but our results show that CO_2 and SO_2 molecules present weak adsorption on these sites. Statistical thermodynamics is applied to obtain the enthalpy, entropy and Gibbs free energy of adsorption for the three molecules onto the available sites at 298 K, which are listed in Table 1. The analysis shows that the adsorptions of both CO_2 and SO_2 on the Mg^{2+} sites are spontaneous processes, whereas their adsorptions onto the Linker sites are not. Alternatively, N_2 does not present any spontaneous adsorption process onto Mg-MOF-74, neither on the Mg^{2+} sites or the Linker sites at 298 K, which explains its low affinity for this adsorbate.

Despite our calculations used to obtain the thermodynamic functions involved a single optimization in a DFT periodic model, which is a simplification of the periodic (DFT) + cluster (MP2/CCSD(T)) method used by Sillar et. al.,[40] our results for the enthalpy and Gibbs free energy of adsorption are in good agreement within the chemical accuracy of 4 kJ/mol at both 298 K and 343 K. This agreement can be seen in Table 2 and validates the simplification of the methodology used to obtain the thermodynamic functions by using only periodic DFT calculations.

The $\Delta G_{i,ads}$ dependence with the gas molecules adsorbed either on the Mg^{2+} sites or on the Linker sites with the Mg^{2+} coverage at several temperatures was also studied, as detailed in Sect. S2 of the Supporting Information. Thermodynamic functions at $\theta_{Mg2+} = 1$ and 298 K are reported in parentheses in Table 1. In general, the Mg^{2+} coverage has a strong effect on the adsorption properties of the Linker sites due to the proximity of these two kinds of sites (i.e., approximately 3.7 Å). On the other hand, the Mg^{2+} coverage have a weaker effect on the Mg^{2+} adsorption properties because the distance between two Mg^{2+}

sites is approximately 7 Å. Concretely, the adsorption on the Linker site is enhanced by the Mg^{2+} coverage, which means that the binding energies and all thermodynamic functions of gas molecules adsorbed on these sites become more negative, also increasing the equilibrium constants of these sites by some orders of magnitude. Finally, notice that when all Mg^{2+} sites are occupied, the Linker/N_2 adsorption site appears as a minimum with a very low equilibrium constant.

3.2 DFT-Based Pure Gas Adsorption Isotherms. DFT/DSL isotherms for pure CO_2, N_2 and SO_2 on Mg-MOF-74 were calculated up to a pressure of 1 atm. The isotherms were built solving eq 3-5 for each pressure at 298 K to compare with previous reported results in the bibliography when available.[26,35,65,66] Note that all experimental adsorption isotherms are measured as excess quantities, whereas our calculations yield the absolute adsorbed amounts. However, this difference is negligible for relatively low pressures (e.g., for CO_2 on Mg-MOF-74 with $P \leq 5$ atm [40]).

It is worth noting that DFT/DSL model gives an upper value of the total adsorption on Mg-MOF-74 due to the assumption that the crystal has all its sites available for adsorption. However, experimentally some sites might be blocked with poisonous species adsorbed during the synthesis, or even defects in the MOF structure that can affect the adsorption site distribution as noted by other authors [40,41,50]. Specifically, depending on the procedure employed for the synthesis of the MOF structure it may yield different adsorption availabilities as proven by Wu et al.[65] For this reason, results from the bibliography for CO_2 adsorption onto Mg-MOF-74 were analysed to derive an average MOF availability to include a scaling factor onto our isotherms, which accounts for this lack of site availability. The scaling factor was validated according to the experimental data of Dietzel et al.,[66] whose results are in very close agreement with the isotherms measured by Mason et al., [26]. On the other hand, Wu et al., used two different procedures to synthesize the Mg-MOF-74. The first procedure yielded adsorption isotherms in good agreement with Dietzel and Mason (data set 1), however, the second procedure produced a highly functional Mg-MOF-74 structure, with a substantially higher total uptake (data set 2). Also, Queen et al., [51] obtained adsorption isotherms in between of the two previous data sets (data set 3). The scaling factor was obtained rescaling our DFT/DSL adsorption isotherms to match the uptake of 8.24 mol/kg of the experimental isotherms, which corresponds to a $\theta = 0.5$ and $\theta_{Mg2+} \approx 1$. Scaling factors were obtained for the three

different experimental data sets at different temperatures when available. Data set 1 showed an average availability of 78.5 % at 293 K, whereas it presented an availability of 83.5% at 343 K. The average availability of this data set is 81.0 %, which is in good agreement with the values derived by Sillar et al., (76.5 %-78.0 %) in their previous works.[40,41,50] Mason performed a fitting of the experimental CO_2 isotherms onto Mg-MOF-74 from 0 to 50 atm with a dual-site Langmuir model, obtaining a Mg^{2+} site saturation parameter of 6.8 mol/kg. For a perfect crystal, the Mg^{2+} site availability is exactly one CO_2 molecule per Mg^{2+} site, which corresponds to 8.24 mol/kg, so the experimental availability calculated by Mason et al. is 82 %, which is also in good agreement with the availability value proposed. In contrast, data set 2 reported only by Wu et al., presented an availability of 93.0 % at a temperature of 298 K. Finally, a site availability of 86.5 % at 298 K was derived from data set 3 of Queen et al., which is slightly above data set 1. Since the majority of results reported in the bibliography have an availability approximately of 81.0 %, only two DFT/DSL isotherms per gas molecule were plot in Figure 3: the perfect crystal isotherm (red lines) and the rescaled isotherm assuming 81 %-availability (blue lines). Two experimental data sets are also shown in Figure 3 for comparison, where our perfect crystal DFT/DLS isotherm lies slightly over the data set 2 from Wu et al., and the 81%-availability isotherm is in good agreement with the data set 1 from Dietzel, Mason and Wu. The results from Queen et al. were not shown for cleanliness.

It should also be noted that the DFT/DSL isotherm is still in good agreement with the experimental uptake of CO_2 at a pressure of 1 atm. This fact confirms the validity of the assumption made in the model neglecting the variation of thermodynamic functions with the Linker coverage. Regarding N_2, DFT/DSL isotherm also accurately reproduces the experimental results from Mason et al.,[26] and Wu et al.,[65] at 298 K. Finally, to our knowledge, reliable experimental results for adsorption isotherms on Mg-MOF-74 are not available in the literature for SO_2.

Our results seem to suggest that the open metal sites are subject to a higher level of poisoning by SO_2, potentially displacing all CO_2 in a hypothetical mixture, which is also deduced from the difference in adsorption energies between these gases (i.e., -46.1 kJ/mol for CO_2 and -78.9 kJ/mol for SO_2, in Table 1). The large SO_2 uptake at low pressures implies that this gas is capable of poisoning Mg-MOF-74, outcompeting CO_2 even in very

low concentrations (e.g., 1,000 ppm). Similar conclusions were also achieved by other studies already published in the literature. [35,63]

DFT/DSL can also provide adsorption isotherms at different temperatures only by changing the temperature in equations of Sect. 2 without requiring further calculations. With this practice, the 81%-availability DFT/DSL isotherms for CO_2 and N_2 were compared with the reliable and extensive experimental data from Mason et al., [26] for temperatures ranging from 293 K to 373 K (see Figure 4). The $\Delta G_{i,ads}$ at different temperatures necessary for building isotherms are reported in Sect. S2 of the Supporting Information. 81%-availability SO_2 isotherm was also obtained, but no reliable experimental data was available to compare with our theoretical results. In general, all isotherms reduce their uptakes with the increase of temperature, but always in a reasonable agreement with reported isotherms. However, instead of using the harmonic approximation for all normal modes in the calculation of adsorbed CO_2 partition functions, some authors considered that the lowest frequency should be accounted as a 1D free rotation to avoid overestimating the entropy loss upon adsorption.[40] This consideration applies at higher temperatures, where adsorbed molecules have enough thermal energy to overcome the rotational barrier of the weakest frustrated rotational mode. The use of a 1D free rotational partition function generally makes the value of $\Delta G_{i,ads}$ more negative, enhancing the gas/adsorbate interactions. In the present work, only the harmonic approximation was considered for simplicity, so it is expected that adsorption isotherms could be somewhat underestimated at very high temperatures because the 1D free rotational mode was not considered.

3.3 Isosteric Heat of Adsorption Analysis. The variation of q_{st} with coverage for each gas at 298 K is shown in Figure 5, calculated by using eq 7 from a single isotherm (also coincident with Clausius-Clapeyron equation using isotherms from 293 K to 313 K to build the isostere). In general, the plot in Figure 5 shows three different regions: i) a low coverage region (i.e., from θ = 0 to θ = 0.3), where q_{st} is almost constant (for instance, $-\Delta H_{Mg,ads} = 44.7$ kJ/mol for CO_2 at zero-coverage, except for the case of SO_2 that depicts a growing trend due to the increase of $-\Delta H_{Mg,ads}$ with the coverage), ii) a high coverage region (i.e., from θ = 0.7 to θ = 1), where q_{st} is constant (e.g., $-\Delta H_{L,ads} = 32.1$ kJ/mol for CO_2 at full Mg^{2+} coverage, because the Mg^{2+} sites are

completely occupied and they stop contributing to the final isosteric heat; iii) an intermediate coverage region (i.e., from $\theta = 0.3$ to $\theta = 0.7$), where the Mg^{2+} sites are close to saturation and the probability of a gas molecule to adsorb onto a Linker site becomes important. This implies that q_{st} gradually decreases from the $-\Delta H_{Mg,ads}$ value onto the $-\Delta H_{L,ads}$ value, until the Mg^{2+} sites are completely saturated. Also, this last region presents an inflection point when the Linker sites become the preferential adsorption sites due to the lack of Mg^{2+} ones, which can be also used as a measure of experimental availability.[51,66]

The results obtained by DFT/DSL model reproduce the experimental q_{st} values for CO_2 at different coverages, including the sigmoidal shape presented by the experimental data of Dietzel et al.[66] and Queen et al.[51] (Figure 5). This inflection point depends on the site availability, showing a clear shift to higher coverages as site availability increases. On the other hand, N_2 presents a low uptake at low and moderate pressures, and for this reason we only have derived the experimental zero-coverage q_{st} of N_2 by using the Clausius-Clapeyron equation (eq 8) with the experimental data of Mason et al. [26], building the isostere with three isotherms at 293 K, 303 K and 313 K. With the available experimental pressure range, q_{st} could only be determined up to $\theta = 0.1$, so only the zero-coverage value was determined (i.e., 22.5/23.5 kJ/mol), in good agreement with the DFT/DSL predicted result. Finally, no experimental data were available for SO_2 but according to our prediction it should present a very high initial q_{st} almost doubling the q_{st} of CO_2 at low coverages.

The present analysis reveals that SO_2 will have the highest affinity for Mg-MOF-74 at any coverage, saturating the Mg^{2+} sites with a very high q_{st} (i.e., from 77.5 to 86.5 kJ/mol) in contrast with CO_2 (i.e., from 44.7 to 42.5 kJ/mol) and N_2 (i.e., from 28.1 to 27.0 kJ/mol), which means that in hypothetical mixtures one should expect that SO_2 will easily poison Mg-MOF-74. After complete saturation of Mg^{2+} sites, the linker sites show again the same trend in q_{st} but with lower absolute values (i.e., 52.8 kJ for SO_2, 32.1 kJ/mol for CO_2 and 12.7 kJ/mol for N_2) the difference between q_{st} for SO_2 and CO_2 is lower in the Linker sites than in Mg^{2+} sites, so although the Linker will also suffer from poisoning, the effect is expected to be lower.

3.4. Impurity Effects and Henry's constants. The adsorption isotherms shown in the previous sections along with the values of the isosteric heats of adsorption demonstrate the great affinity of Mg-MOF-74 for SO_2, according to the ranking $SO_2 > CO_2 > N_2$. However, in mixtures where low partial pressures of impurities (e.g., SO_2) are present, the main parameter that gives information about the rate of poisoning with pollutants is the ratio between the Henry's constants of CO_2 and the impurity. The Henry's constant is the equilibrium constant of the Langmuir isotherm in the low-pressure limit, where the Langmuir expression reduces to a linear expression (i.e., $\theta \approx K_H P$). Notice that the term $K_L(\theta)P$ in eq 3 will be negligible as the equilibrium constant for the adsorption on a Mg^{2+} site is significantly larger than the one on the Linker site, so the Henry's constant for each gas is defined as the zero-coverage K_{Mg2+}. This magnitude is directly related to the adsorbate/substrate affinity, which makes important the analysis of Henry's constant differences between the desired product (i.e., CO_2) and the impurities (i.e., SO_2), trying to find the optimal working temperature, where CO_2 selectivity [11] is maximized with respect to SO_2.

Figure 6 shows the evolution of Henry's constants with temperature, as obtained from the DFT/DSL model, for CO_2 adsorption compared with N_2 and SO_2. As it can be seen, Henry's constant for CO_2 is high enough to be selectively adsorbed onto Mg-MOF-74 in a binary mixture with N_2, but it is not high enough to prevent poisoning from SO_2. However, the CO_2/SO_2 Henry's ratio increases monotonically with temperature. This implies that high temperatures could improve the Mg-MOF-74 selectivity towards CO_2 in a mixture with SO_2. Since from CO_2 and SO_2 isotherms (Figure 3) can be concluded that desorption of CO_2 (e.g., by decreasing pressure) is less energy intensive than for SO_2, an optimal separation of both gases implies a major adsorption of CO_2 onto the Mg-MOF-74. Therefore, working at very high temperatures is advisable (Figure 6), but it would also lead to a lower overall uptake, decreasing the effectiveness of this material towards CO_2 capture (Figure 4). To compare the limit cases studied, Henry's constants of CO_2 and SO_2 are approximately 26 and 53,600 1/atm, respectively, at 293 K, and 0.5 and 38 1/atm at 373 K. These values mean that the affinity of Mg-MOF-74 for SO_2 is more than 2,061 times higher than for CO_2 at 293 K, whereas it is only 76 times higher at 393 K. On the other hand, the total uptake of CO_2 when increasing temperature is approximately reduced from 8.5 mol/kg at 293 K to 3.5 mol/kg at 393 K. However, as the Henry's constants ratio improves CO_2 separation more rapidly than the decrease of uptake with

temperature rise, the best separation of CO_2 in a mixture containing SO_2 traces will be at higher temperatures (i.e., > 373 K according to our analysis). Nevertheless, the efficiency of this separation will be very low because at any studied temperature SO_2 Henry's constant is higher than CO_2, so Mg-MOF-74 still preferentially adsorbs SO_2. For this reason, it is strongly recommended to remove SO_2 from a post-combustion flue gas mixture before employing Mg-MOF-74 as adsorbent material for CO_2 capture and separation.

3.5. Study of SO_2 Effects in CO_2 separation from Gas Mixtures using Mg-MOF-74. The typical temperature and pressure conditions for a post-combustion flue gas are 313-333 K and 1 atm, respectively,[67] with a composition for a coal-fired power plant containing 70–75% N_2, 15% CO_2, 3-4 % O_2, 5–7% water and traces of other species [68] (500 ppm NO_x and up to 2,000 ppm SO_2 when burning high-sulphur coals [69]). The SO_2 poisoning effect onto Mg-MOF-74 was evaluated assuming a ternary mixture containing CO_2, N_2 and SO_2. The total uptake of the three gases at a total pressure of 1 atm was compared for different SO_2 impurity concentrations, which varied from a few tenths ppm up to 1 mol %, maintaining CO_2 in 15% and N_2 as the surplus. It was assumed that the complex flue gas mixture does not contain water because it was dried in a previous step before adsorption, and O_2 was neglected because it behaves very similar to N_2 when adsorbed onto MOFs, according to previous reported results. [35,70]

The total uptake of CO_2, N_2 and SO_2 was evaluated by varying the percentage traces of SO_2, using a multicomponent dual-site Langmuir model for gas mixtures based on DFT/DSL model. Thus, the equilibrium coverage of a species (θ_j) at a partial pressure P_j in a ternary mixture with j = CO_2, N_2 or SO_2 is calculated by using eq 10. As this expression only refers to the coverage of a single species, but it depends on the coverage of the three components of the mixture, three equations (one for species) have to be solved simultaneously in an iterative process until convergence of the three coverages.

$$\theta_j = \chi_{Mg2+}\theta_{j,Mg2+} + \chi_L\theta_{j,L} =$$

$$= \chi_{Mg2+}\frac{K_{j,Mg2+}(\theta_j)P_j}{1+\sum_{j=CO_2,N_2,SO_2}[K_{j,Mg2+}(\theta_j)\,P_j]} + \chi_L\frac{K_{j,L}(\theta_j)\,P_j}{1+\sum_{j=CO_2,N_2,SO_2}[K_{j,L}(\theta_j)\,P_j]} \qquad (10)$$

The multicomponent DFT/DSL model of eq 10 implicitly considers the thermodynamic equilibrium competition between different species for each adsorption site. However, the DFT/DSL model is currently developed for single species because it only considers the effect of Mg^{2+} coverage between molecules of the same gas species (i.e., the interactions between molecules of the same type). This implies that some lateral interactions are still missing in this model (i.e., the interactions between molecules of different type), which may lead to small deviations in the region where the there are two or more gases with non-negligible adsorption. Although future efforts in building the complete set of interactions would refine the model (i.e., obtaining the variation of $\Delta G_{i,ads}$ with the coverage of different species), the main results are expected not to change significantly due to the large difference in SO_2/CO_2 affinity for the Mg-MOF-74.

Figure 7 shows the isotherms of different ternary mixtures calculated at 313 K with eq 10. Three concentrations were selected to show the behaviour of the gas adsorption with the presence of SO_2 impurities at conditions where i) SO_2 is too diluted to affect CO_2 adsorption (e.g., 0.005% SO_2), ii) SO_2 is at a concentration capable of affecting some sites in Mg-MOF-74 (e.g., 0.02% SO_2) and iii) SO_2 concentration is high enough to almost completely poison Mg-MOF-74 (e.g., 0.1% SO_2). As it can be seen, at impurity concentrations close to 0.02% the SO_2 uptake is very similar to the CO_2 uptake, so even at this low concentration, SO_2 strongly competes with CO_2, whereas N_2 uptake remain close to zero at all SO_2 concentrations. To locate the exact concentration of SO_2 in the flue gas mixture that surpasses CO_2 in uptake, several adsorption isotherms in perfect crystal Mg-MOF-74 were calculated for different % SO_2. The uptake at a total pressure of 1 atm for different % SO_2 are collected in Figure 8, where we observe that CO_2 content in Mg-MOF-74 decreases when increasing SO_2 percentage, with a negligible N_2 adsorption in all range. The change of adsorption behaviour (i.e., when Mg-MOF-74 adsorbs more SO_2 than CO_2) occurs in a reduced range of concentrations, being the crossing point between the CO_2 and SO_2 uptakes approximately at 0.020/0.025 % SO_2 at 313 K. However, these results are affected by temperature, as it can be seen also in Figure 8, where the uptake at 1 atm and 353 K is significantly lower for all gases than the uptake at 313 K. The crossing point between CO_2/SO_2 uptake also moves onto higher % SO_2 denoting an increase of CO_2-over-SO_2 selectivity when increasing temperature. For this reason, additional work was made to analyse the effect of SO_2 poisoning with temperature. Similar plots to Figure 8 were built using the multicomponent DFT/DSL

model from 293 K up to 373 K and the % CO_2 in the adsorbed phase was analysed. The results are collected in Figure 9, where the low temperature / low % SO_2 region presents the highest % of adsorbed CO_2. Increasing temperature reduces CO_2 adsorption, up to 75-50% at higher temperatures. On the other hand, increasing % SO_2 in the gas mixture reduces enormously the % CO_2 in the adsorbed phase; for example, at 313 K and 0.002% SO_2 presents a % CO_2 higher than 90% whereas at 313 K and 0.02% SO_2 the % CO_2 is reduced to approximately 50%.

3.6. Analysis of some Swing Adsorption Techniques for Optimal CO_2 Separation. The previous section treated the effect of SO_2 as an impurity of a CO_2/N_2 mixture in an adsorption process on Mg-MOF-74, showing that a low concentration of SO_2 in the flue gas mixture (i.e., e.g., 0.020/0.025 % SO_2 at 313 K) was enough to significantly adsorb more SO_2 than CO_2. However, in commercial gas separation/purification processes a regeneration of the sorbent bed is required for reuse in further adsorption cycles.[26,71,72,73] These cycles are typically accomplished with a desorption step, where not all adsorbed gases can be effectively desorbed, performed by i) decreasing pressure (Pressure Swing Adsorption, PSA, or Vacuum Swing Adsorption, VSA), ii) increasing temperature (Temperature Swing Adsorption, TSA) or iii) by application of electrical current (Electric Swing Adsorption, ESA). Among these methods, TSA and VSA are particularly promising processes for post-combustion CO_2 capture, owing to difficulties with compressing large volumes of flue gas streams.[26,74]

In VSA the standard adsorption/desorption cycle is done at constant temperature (e.g., 313 K) but decreasing the pressure from 1 atm (adsorption pressure) to about 0.1 atm (desorption pressure). However, in TSA the standard cycle is done at constant pressure (e.g., 1 atm) but increasing temperature from 313 K (adsorption temperature) to 373-443 K (desorption temperature). In this section, we analysed these methods, considering VSA cycle from 1 atm (adsorption pressure) to 0.1 atm (desorption pressure) and TSA from 313 K (adsorption temperature) to 373 K (desorption temperature). These two cycles can also be combined onto a VTSA process where the adsorption is done at 1 atm and 313 K and the desorption process is carried out 0.1 atm and 373 K (i.e., from atmospheric pressure and low temperature to low pressure and high temperature).

Two different evaluation criteria were considered in this work to analyze the CO_2 recovery performance in such swing adsorption processes: i) the working capacity and ii)

the composition of the outlet mixture. The former represents the amount of gas (e.g., CO_2) that can be recovered after an adsorption/desorption cycle. This parameter is generally more relevant than the total uptake at the adsorption pressure, because not all the gas adsorbed onto a material can be effectively recovered. The working capacity (W_j) of a selected component in the mixture (e.g., CO_2) is calculated from the difference between the equilibrium uptake under adsorption and desorption conditions. The adsorption value can be obtained directly from uptake at 1 atm and 313 K of the mixture calculation and the desorption value is obtained by multiplying the pure uptake at desorption conditions by the composition in the adsorbed phase, as done in our previous work.[11] This approach is necessary for high SO_2 content, where impurity uptakes are not negligible, and allows more realistic results than those found in the literature based on pure adsorption data.[26,75]

Figure 10 shows the CO_2 working capacities for the selected TSA, VSA and VTSA processes as a function of the % SO_2 at the inlet mixture. The black line in Figure 10 represents the maximum working capacity of CO_2 that can be accomplished, which coincides with the total uptake in Mg-MOF-74 at 313 K and 1 atm. The VSA process recovers only 1 mol/kg of CO_2 per adsorption/desorption cycle at 0.001% SO_2 in contrast to the 6.4 mol/kg of the ideal maximum recovery. The TSA process recovers around 2 mol/kg of CO_2 per cycle, which is substantially higher than the VSA, but not efficient enough to accomplish CO_2 recovery from Mg-MOF-74. Finally, the VTSA presents a very high working capacity (i.e., 5.9 mol/kg of CO_2 per cycle at 0.001% SO_2), which means that over 90% of adsorbed CO_2 can be effectively recovered. All working capacities, as well as the ideal maximum recovery, are reduced by the % SO_2 at the inlet mixture, but the relative behaviours among the three processes remain equivalent, making VTSA a promising technique for this material.

On the other hand, the composition of the outlet mixture (i.e., purity) is an important variable to consider, especially when is possible to reuse the captured CO_2 for other applications. The composition at the outlet: Y_j^{out} (do not confuse with the composition in the adsorbed phase: Y_j^{ads}, or the composition at the inlet: Y_j^{in}) can be calculated as the relationship between working capacity of the desired component and the sum of working capacities of all components in the mixture (eq. 11).[6]

$$Y_j^{out} = W_j / \sum_{i=CO_2,N_2,SO_2} W_i \qquad (11)$$

In Figure 11, the composition of the outlet stream as a function of the % SO_2 at the inlet can be seen for the three-selected adsorption/desorption processes. VSA is the cycle that presents the lowest $Y_{CO_2}^{out}$ along the whole range of $Y_{SO_2}^{in}$, and its purity is reduced when increasing the amount of SO_2 at the inlet mixture. However, $Y_{SO_2}^{out}$ will be zero in most cases because this gas has a very strong affinity for Mg-MOF-74 and once adsorbed it cannot be desorbed by only reducing pressure up to 0.1 atm. On the other hand, TSA yields a higher CO_2 purity, but the outlet starts containing important amounts of SO_2 at $Y_{SO_2}^{in}$ > 0.2%. Finally, the studied VTSA process presents the highest $Y_{CO_2}^{out}$ at low $Y_{SO_2}^{in}$, which remains almost constant up to 0.03% SO_2 at the inlet mixture. At higher $Y_{SO_2}^{in}$ the VTSA outlet stream becomes strongly poisoned by SO_2 making impossible the CO_2 recovery for further processes.

This analysis shows that VTSA is the most promising cycle at the studied conditions, being around three times more effective than TSA or six times more effective than VSA, regarding working capacities. Even though VTSA is the most expensive process, because it includes a TSA combined with a VSA cycle, the recovery is very large in comparison to the other cycles. With regard to the purity, VTSA also presents the largest $Y_{CO_2}^{out}$ with values close to 95% of CO_2 up to $Y_{SO_2}^{in}$= 0.03%. For higher amounts of $Y_{SO_2}^{in}$ TSA is preferable up to 0.3% SO_2 and VSA for $Y_{SO_2}^{in}$ > 0.3%. However, the working capacities at these SO_2 concentrations are too low to be effectively used in CO_2 separation.

It is important to notice that although the % of adsorbed CO_2 on Mg-MOF-74 ($Y_{CO_2}^{ads}$) at $Y_{SO_2}^{in}$= 0.03% and 313 K is approximately 30% (Figure 9), the VTSA outlet stream contains a 95% of CO_2 (Figure 11) and a 5% of N_2 (i.e., 95% purity). This means that CO_2 could be successfully recovered and separated from the flue gas mixture using VTSA if $Y_{SO_2}^{in} \leq$ 0.03% even if the MOF structure contains a large amount of SO_2, because it is not desorbed at the desorption step.

4. CONCLUSIONS

This work studies the adsorption of some pure cases (i.e., CO_2, N_2 and SO_2) on Mg-MOF-74 absorbent, developing a dual-site Langmuir model based on own periodic DFT calculations and a mean-field approximation for the inclusion of the lateral interactions, considering the effect of the surface coverage in the thermodynamic functions of adsorption. Our model, although simplified in the use of DFT data, presents adsorption isotherms and isosteric heats of adsorption in good agreement with available experimental data and with previous more accurate but also more complex ab initio models.

An extension of this model to treat gas mixtures is also presented and applied to post-combustion gases (i.e., $CO_2/N_2/SO_2$), considering the effect of SO_2 as impurity. It was shown that SO_2 concentrations as low as 0.02% in the flue gas mixture are enough to achieve higher uptakes than CO_2 on Mg-MOF-74 at 313 K. This low concentration slightly increased with temperature, allowing us to obtain the optimal working conditions where Mg-MOF-74 can still adsorb mainly CO_2 as a function of temperature and pollutant concentration.

Three different swing adsorption processes (i.e., TSA, VSA and VTSA) were analysed to determine the efficiency of the adsorption/desorption cycle through working capacities and the purity of the recovered CO_2. It was shown how VTSA outperforms the selected TSA and VSA cycles in both properties, especially at low % of SO_2 in the flue gas mixture. High amounts of SO_2 reduce the working capacity of CO_2 as well as its purity at the outlet, making unpractical CO_2 recovery with Mg-MOF-74.

Finally, future work should be devoted to build a more complex model in order to obtain multicomponent DFT/DSL mixture isotherms, which account for the complete set of crossed lateral interactions between all species in the mixture. Also, additional species should be studied (e.g., O_2, NO_2, NO,…) and their poisoning effects in post-combustion flue gas mixtures.

▪ ASSOCIATED CONTENT

*** Supporting Information**

Details of the determination of thermodynamic functions by using DFT calculations and statistical thermodynamics. $\Delta G_{i,ads}$ dependence with temperature at zero-coverage and full Mg^{2+} coverage.

▪ AUTHOR INFORMATION

Corresponding Author

*E-mail address: r.sayos@ub.edu (Ramón Sayós). Phone.: +34 934 034 760.

ORCID

Gerard Alonso: 0000-0001-8162-9270

Daniel Bahamon: 0000-0001-5473-1202

Fatemeh Keshavarz: 0000-0003-2189-7809

Xavier Giménez: 0000-0002-7003-1713

Pablo Gamallo: 0000-0002-8531-8063

Ramón Sayós: 0000-0001-6627-7844

NOTES

The authors declare no competing financial interest.

▪ ACKNOWLEDGMENTS

Financial support to this research has been provided by the Spanish Ministry of Economy and Competitiveness (project number CTQ2014-53987-R) and, in part, from the Generalitat de Catalunya (project number 2014SGR1582). G.A. thanks University of Barcelona for a predoctoral APIF-2016 grant and P.G. thanks Generalitat de Catalunya for his Serra Húnter Associate Professorship. F.K. acknowledges the Financial support from Ministry of Science, Research and Technology of Iran (Ref: 215431).

Tables

Table 1. Zero-coverage DFT adsorption energies, thermodynamic functions and equilibrium constants derived from single CO_2, N_2 and SO_2 molecule adsorption processes on both Mg^{2+} and Linker sites. The values in parentheses were obtained considering the effect of Mg^{2+} full coverage for both i = Mg^{2+} and i = Linker sites. All values are shown in kJ/mol at a temperature of 298 K, except the equilibrium constant which has units of 1/atm.

	CO_2		N_2		SO_2	
	Mg^{2+}	Linker	Mg^{2+}	Linker	Mg^{2+}	Linker
$\Delta E_{i,ads}$	-47.9 (-47.0)	-30.4 (-35.1)	-32.2 (-33.4)	N/A (-16.4)	-81.5 (-86.4)	-38.6 (-57.0)
$\Delta E_{i,ads}$ (with ZPE)	-46.1 (-45.6)	-29.5 (-34.5)	-29.3 (-30.5)	N/A (-15.0)	-78.9 (-83.8)	-36.6 (-55.1)
$\Delta U_{i,ads}$	-42.2 (-41.4)	-24.9 (-29.6)	-25.6 (-26.8)	N/A (-10.2)	-75.0 (-80.0)	-31.7 (-50.3)
$\Delta H_{i,ads}$	-44.7 (-43.9)	-27.4 (-32.1)	-28.1 (-29.3)	N/A (-12.7)	-77.5 (-82.5)	-34.2 (-52.8)
$T\Delta S_{i,ads}$	-37.4 (-33.2)	-33.7 (-34.3)	-32.2 (-31.2)	N/A (-24.6)	-52.1 (-54.0)	-51.3 (-51.3)
$\Delta G_{i,ads}$	-7.3 (-10.7)	6.3 (2.2)	4.1 (1.9)	N/A (11.9)	-25.6 (-28.5)	17.1 (-1.5)
K_i	19.25(75.63)	0.0773(0.4099)	0.1931(0.4576)	0.0 (0.0083)	30493.5(97757.8)	0.0010(1.8315)

Table 2. Enthalpy and Gibbs free energy of adsorption of a CO_2 molecule in the Mg^{2+} and Linker sites at zero-coverage and two temperatures (i.e., 298 K and 343 K) obtained by periodic DFT calculations in comparison to the same magnitudes calculated by Sillar et. al., [40] (in parentheses). All results are in agreement within the chemical accuracy of 4 kJ/mol.

	CO_2 at 298 K		CO_2 at 343 K	
	Mg^{2+}	Linker	Mg^{2+}	Linker
ΔH_{ads}	-44.7 (-46.1)	-27.4 (-30.4)	-44.2 (-45.7)	-26.8 (-30.0)
ΔG_{ads}	-7.3 (-9.2)	6.3 (5.1)	-1.7 (-3.7)	11.4 (10.4)

Figures

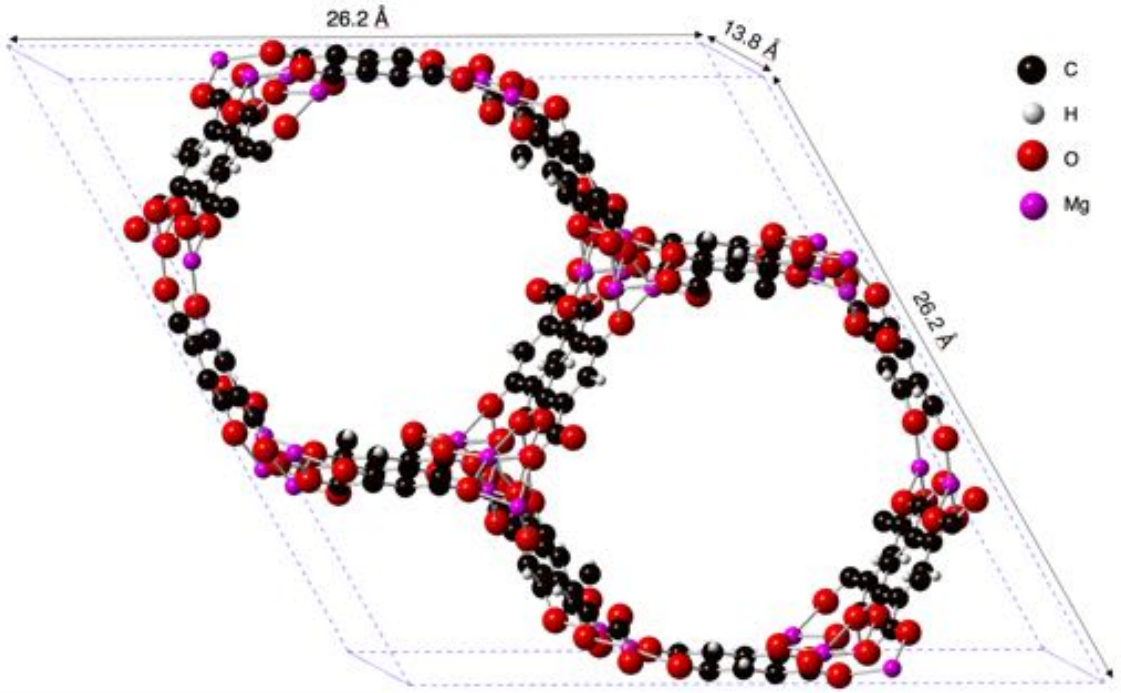

Figure 1. Fully relaxed structure of Mg-MOF-74 optimized by the periodic DFT calculations.

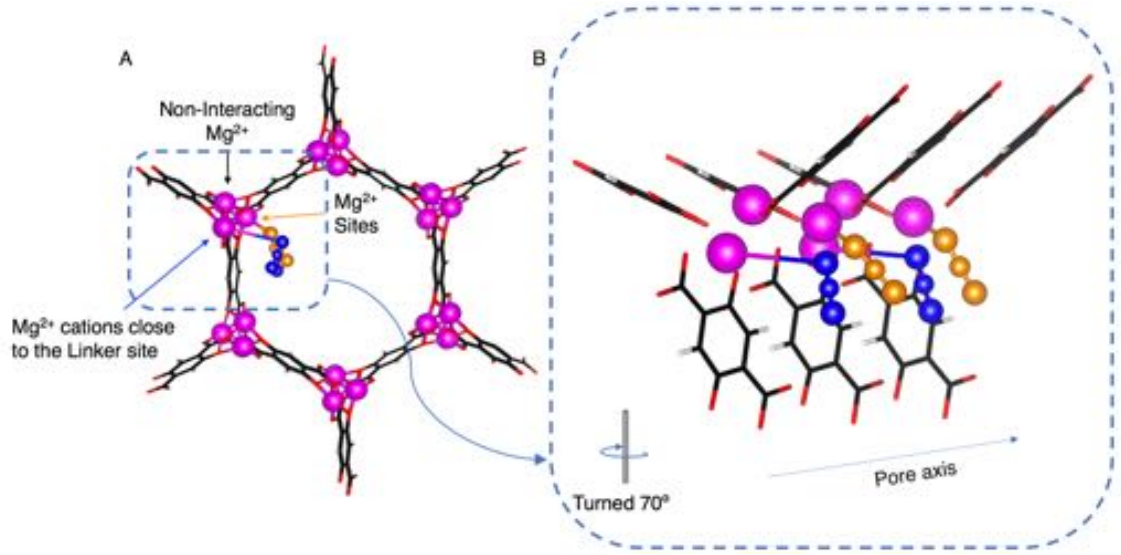

Figure 2. (a) Representation of a Mg-MOF-74 pore, where two CO_2 molecules (in orange) are adsorbed onto the Mg^{2+} sites and two CO_2 molecules (in blue) are adsorbed onto the Linker sites, which also weakly interact with a Mg^{2+} cation stabilizing the adsorption site. The squared region in (A) is zoomed in (B) and slightly turned to see that the adsorption site distribution is alternated (i.e., Linker-Mg^{2+}-Linker-Mg^{2+}).

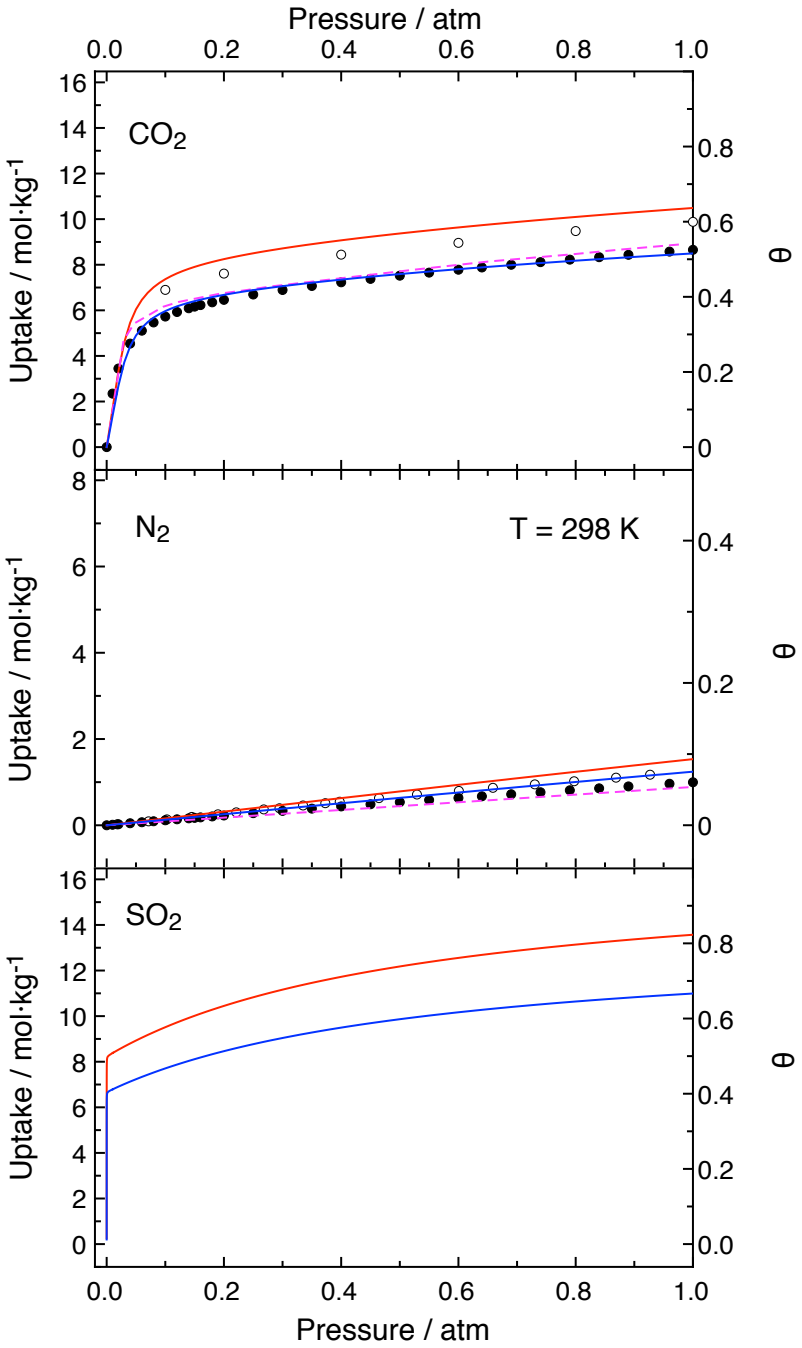

Figure 3. Adsorption isotherms predicted for pure CO_2 (Top), N_2 (Middle) and SO_2 (Bottom) on Mg-MOF-74. DFT/DSL isotherms accounting for lateral interactions are represented in solid lines: red for the perfect crystal and blue for 81%-availability isotherm. Results from Sillar et al., [40,41] with the more complex model are given for validation (in dashed magenta). Also, experimental results from data set 1 (•) [26,65,66] and data set 2 (○) [65] are used to compare CO_2 and N_2 isotherms at 298 K.

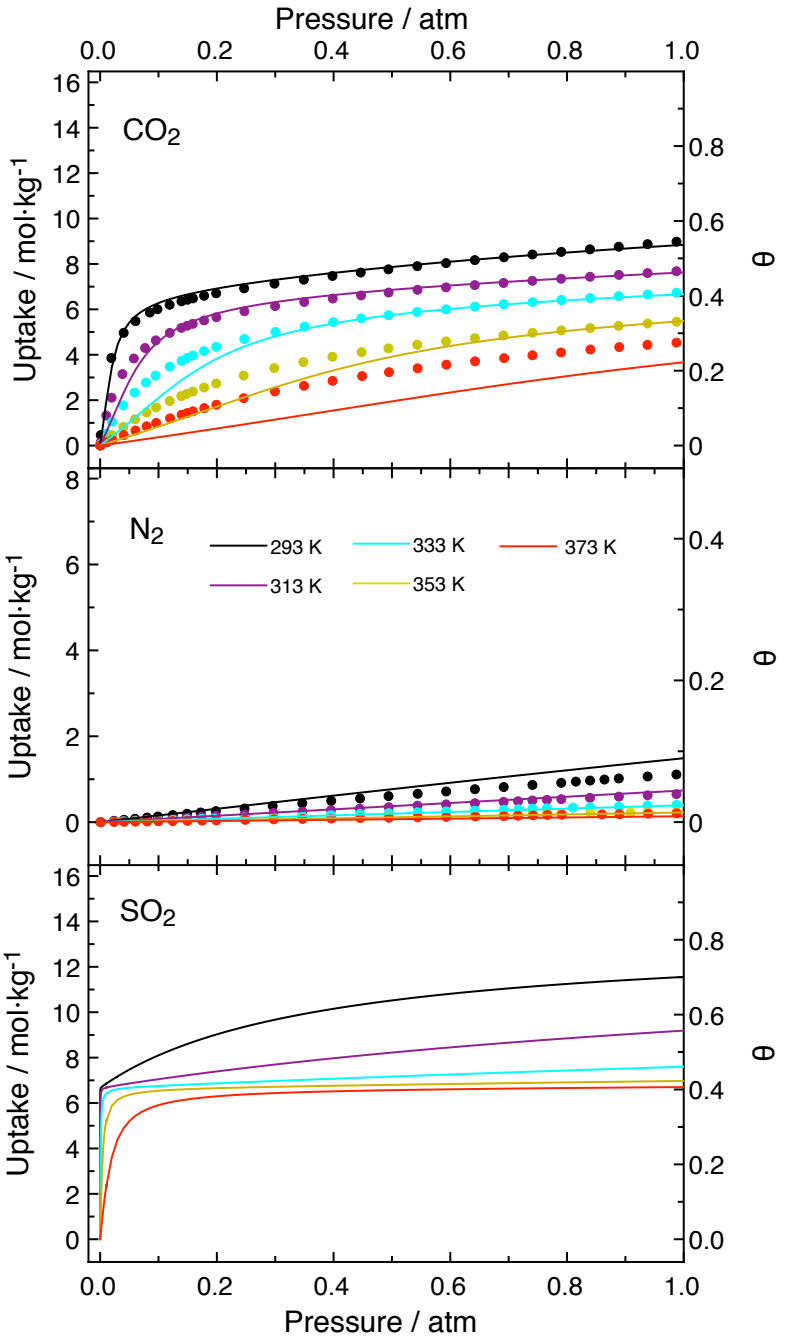

Figure 4. Temperature effect on the pure component 81%-availability DFT/DLS adsorption isotherms (solid lines) compared with experimental results from Mason et al., [26] (dots). Different colours represent different temperatures ranging from 293 K to 373 K.

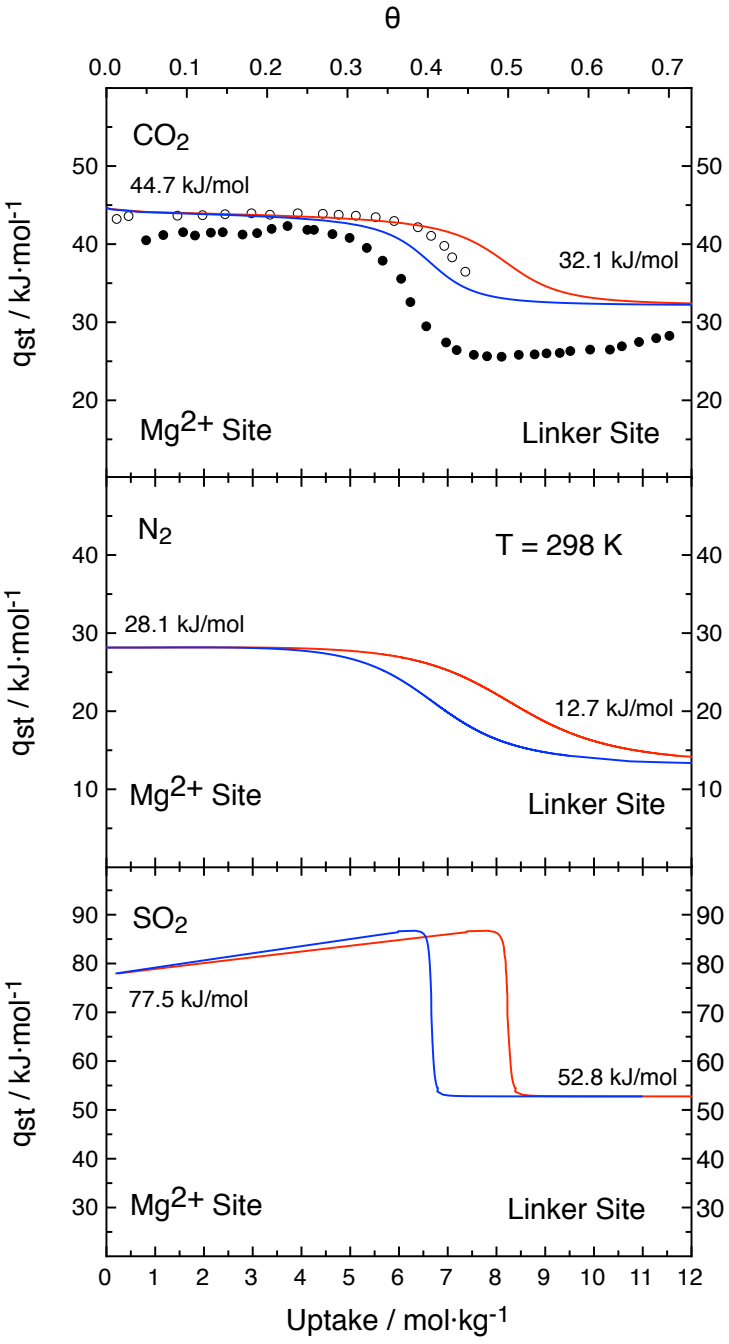

Figure 5. DFT/DSL variation of isosteric heat of adsorption (q_{st}) with coverage for a perfect crystal (red), 81%-availability of sites (blue) for CO_2, N_2 and SO_2 obtained with eq 7. The results obtained with Clausius-Clapeyron equation (eq 8) are not shown because they are almost identical to the ones obtained by eq 7. Experimental reported results of Dietzel et al., (•) [66] and Queen et al., (○) [51] are indicated when available for comparison.

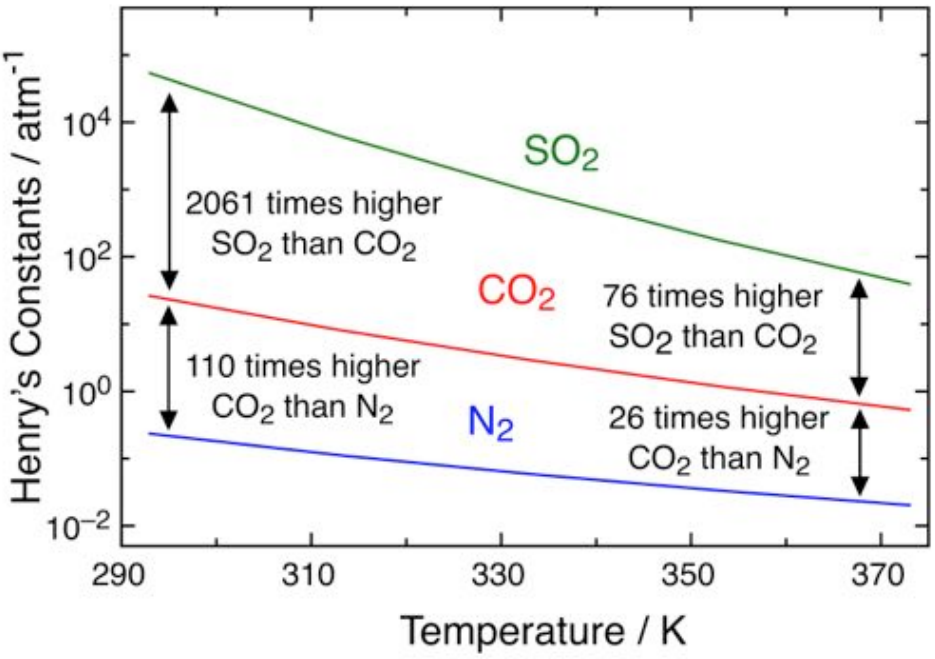

Figure 6. CO_2, N_2 and SO_2 Henry's constants at different temperatures from 293 K to 373 K, where the reduction of SO_2 affinity towards Mg-MOF-74 can be observed.

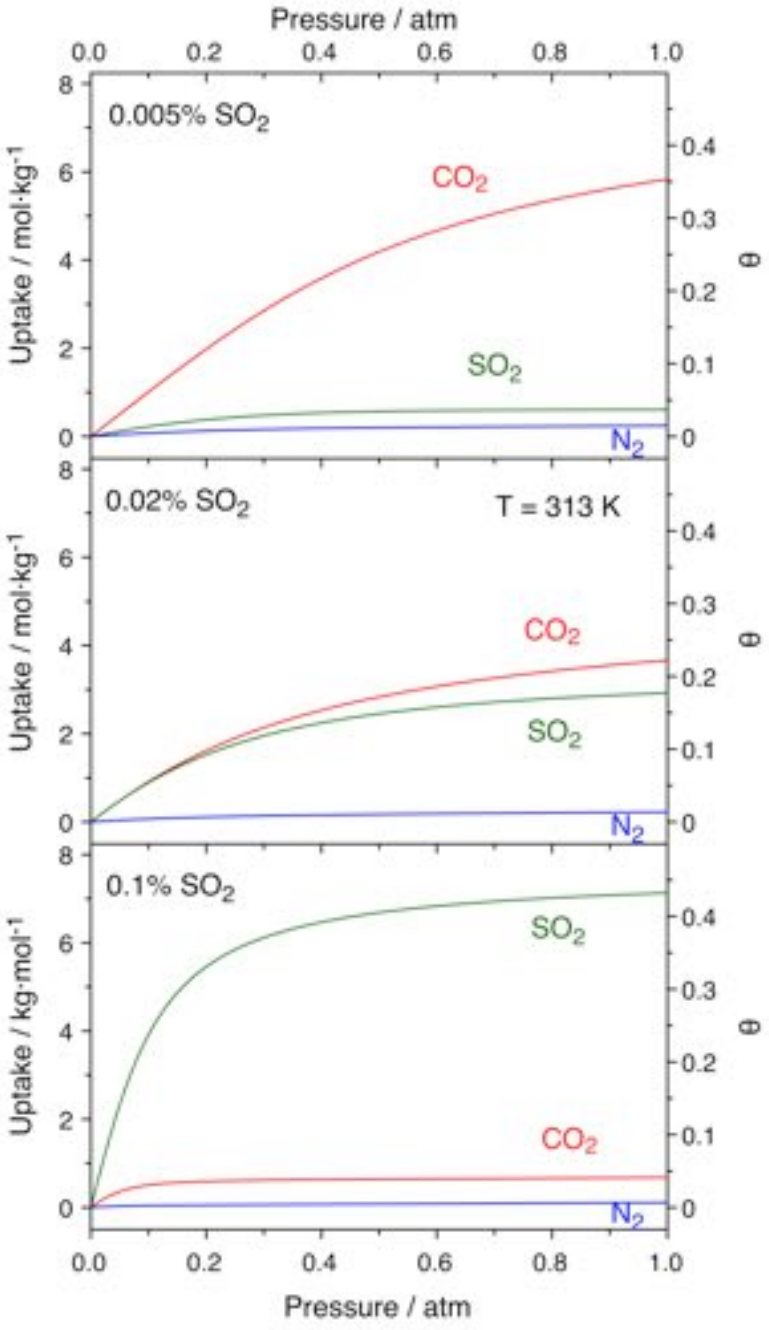

Figure 7. DFT/DSL isotherms for the ternary mixture obtained with the multi-component dual-site Langmuir model (eq 10) at 313 K with three different initial SO_2 concentrations (i.e., from lower concentration at top, to higher concentration at bottom) keeping CO_2 at 15% and N_2 as the surplus.

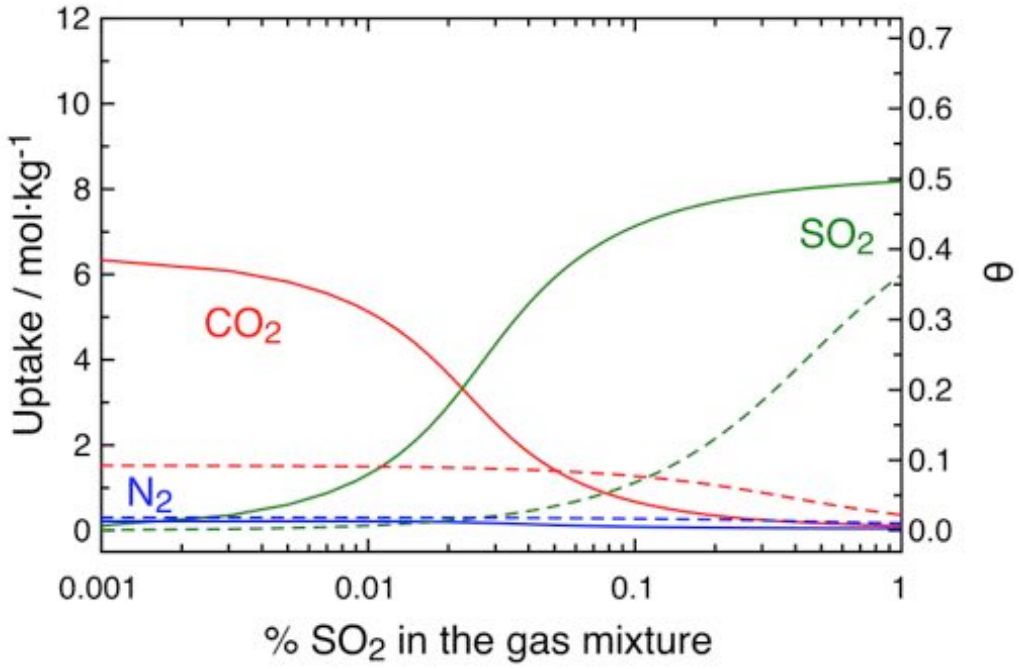

Figure 8. Calculated gas adsorption uptake at different mol % SO_2 in ternary gas mixtures with 15% CO_2, and N_2 as the surplus. DFT/DSL model results were obtained with the multicomponent dual-site Langmuir model (eq 10). The results are shown at 313 K (solid lines) according to a typical post-combustion flue gas temperature and at 353 K (dashed lines) to analyse the temperature effect on the CO_2/SO_2 uptake.

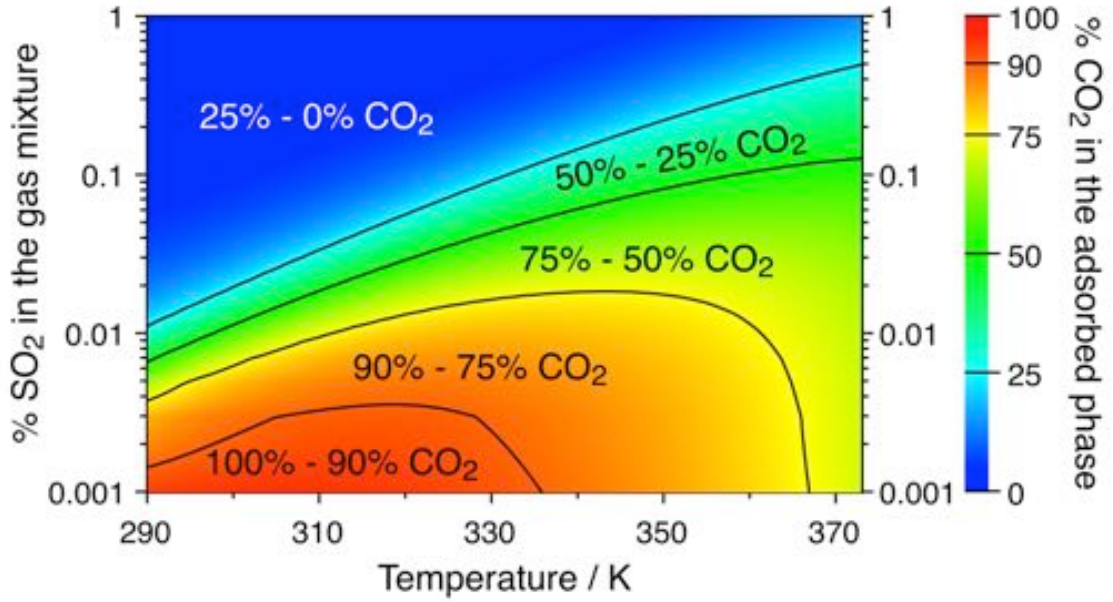

Figure 9. Variation of the % CO_2 in the adsorbed phase at different temperatures and SO_2 concentrations of the flue gas. The red region shows the conditions where almost the whole structure is occupied by CO_2, whereas green and blue regions show where SO_2 importantly affects the CO_2 adsorption (i.e., close or past the crossing CO_2/SO_2 point in Figure 8).

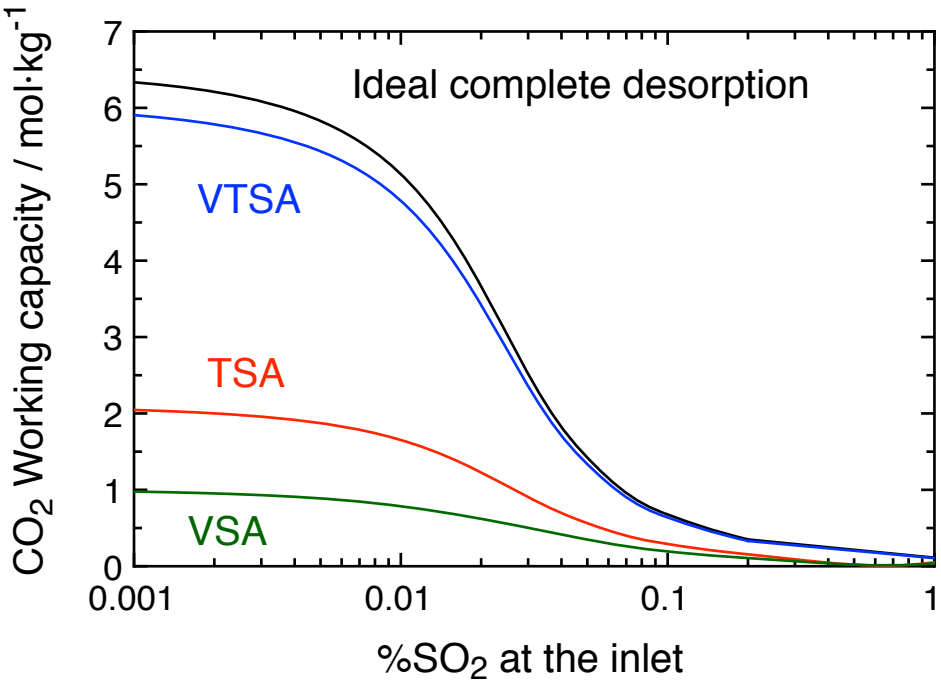

Figure 10. CO_2 Working capacities for the selected VSA (green), TSA (red) and VTSA (blue) processes as a function of % SO_2 in the inlet flue gas at 313 K. The black line corresponds to the ideal situation where all CO_2 adsorbed on the structure would be desorbed, that is, the CO_2 uptake shown in Figure 8 at 313 K.

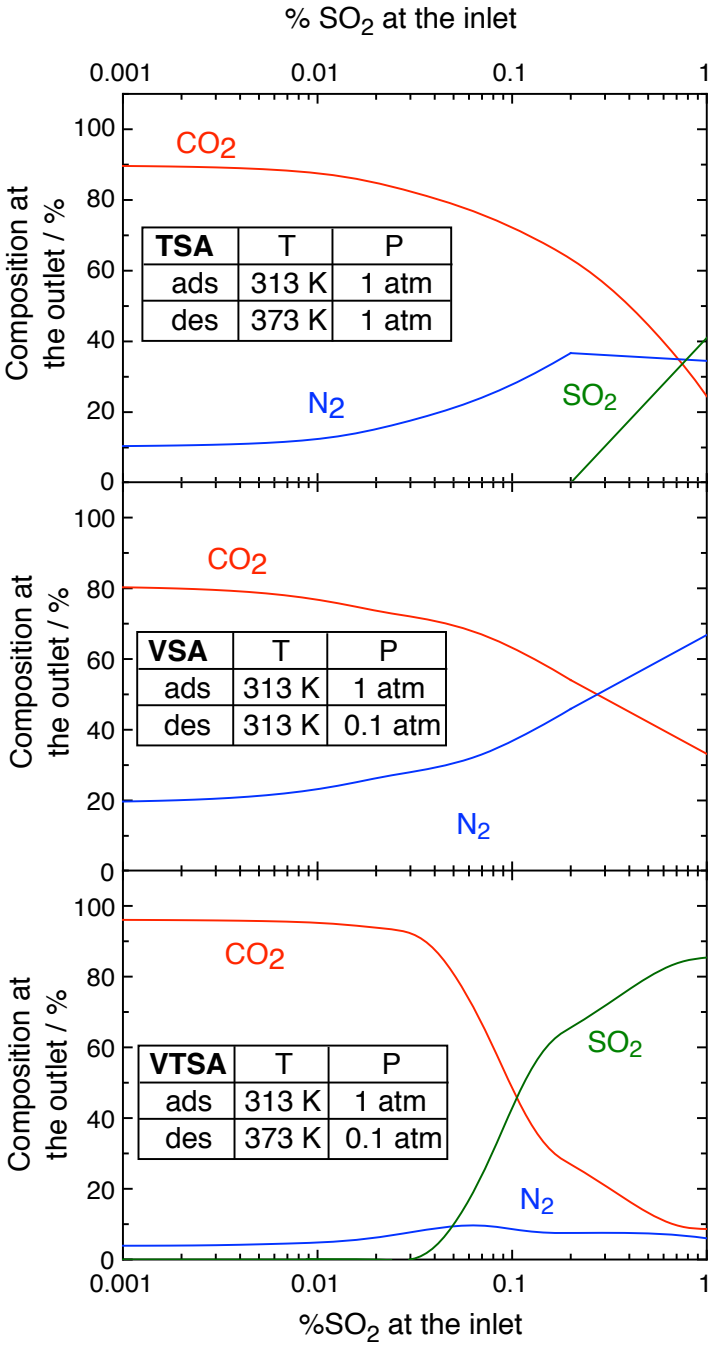

Figure 11. CO_2, N_2 and SO_2 composition at the outlet stream as a function of the % SO_2 in the inlet flue gas mixture for the selected TSA (top), VSA (middle) and VTSA (bottom) processes. The adsorption/desorption conditions can be seen in each graph.

References

(1) Zou, R.; Abdel-Fattah, A. I.; Xu, H.; Zhao, Y.; Hickmott, D. D. Storage and Separation Applications of Nanoporous Metal–Organic Frameworks. *Cryst. Eng. Comm.* **2010**, *12*, 1337-1353.

(2) White, C. M.; Strazisar, B. R.; Granite, E. J.; Hoffman, J. S.; Pennline, H. W. Separation and Capture of CO_2 from Large Stationary Sources and Sequestration in Geological Formations-Coalbeds and Deep Saline Aquifers. *J. Air Waste Manage. Assoc.* **2003**, *53*, 645-715.

(3) MacDowell, N.; Florin, N.; Buchard, A.; Hallett, J.; Galindo, A.; Jackson, G.; Adjiman, C. S.; Williams, C. K.; Shah, N.; Fennell, P. An Overview of CO_2 Capture Technologies. *Energy Environ. Sci.* **2010**, *3*, 1645-1669.

(4) Rao, A. B.; Rubin, E. S. A Technical, Economic, and Environmental Assessment of Amine-Based CO_2 Capture Technology for Power Plant Greenhouse Gas Control. *Environm. Sci. & Tech.* **2002**, *36*, 4467-4475.

(5) Sumida, K.; Rogow, D. L.; Mason, J. A.; McDonald, T. M.; Bloch, E. D.; Herm, Z. R.; Bae, T. H.; Long, J. R. Carbon Dioxide Capture in Metal–Organic Frameworks. *Chem. Rev*. **2012**, *112*, 724-781.

(6) Huck, J. M.; Lin, L.-C.; Berger, A. H.; Shahrak, M. N.; Martin, R. L.; Bhown, A. S.; Haranczyk, M.; Reuter, K.; Smit, B. Evaluating Different Classes of Porous Materials for Carbon Capture. *Energy Environ. Sci.* **2014**, *7*, 4132-4146.

(7) Matito-Martos, I.; Martin-Calvo, A.; Gutierrez-Sevillano, J. J.; Haranczyk, M.; Doblare, M.; Parra, J. B.; Ania, C. O.; Calero, S. Zeolite Screening for the Separation of Gas Mixtures Containing SO_2, CO_2 and CO, *Phys. Chem. Chem. Phys*. **2014**, *16*, 19884-19893.

(8) Damen, K.; van Troost, M.; Faaij, A.; Turkenburg, W. A. Comparison of Electricity and Hydrogen Production Systems with CO_2 Capture and Storage. Part A: Review and Selection of Promising Conversion and Capture Technologies. *Prog. Energy Combust. Sci*. **2006**, *32*, 215-246.

(9) Bhown, A.; Freeman, B. Analysis and Status of Post-Combustion Carbon Dioxide Capture Technologies. *Environ. Sci. Technol.* **2011**, *45*, 8624-8632.

(10) Lin, L.; Berger, A. H.; Martin, R. L.; Kim, J.; Swisher, J. A.; Jariwala, K.; Rycroft, C. H.; Bhown, A. S.; Deem, M. W.; Haranczyk, M.; Smit, B. In Silico Screening of Carbon-Capture Materials. *Nat. Mater*. **2012**, *11*, 633-641.

(11) Prats, H.; Bahamon, D.; Alonso, G.; Giménez, X.; Gamallo, P.; Sayós, R. Optimal Faujasite Structures for Post-Combustion CO_2 Capture and Separation in Different Swing Adsorption Processes. *J. CO_2 Util*. **2017**, *19*, 100-111.

(12) Bahamon, D.; Vega, L. F. Systematic Evaluation of Materials for Post-Combustion CO_2 Capture in a Temperature Swing Adsorption Process. *Chem. Eng. J.* **2016**, *284*, 438-447.

(13) Prats, H.; Bahamon, D.; Giménez, X.; Gamallo, P.; Sayós, R. Computational Simulation Study of Faujasite Si/Al Ratio on CO_2 Capture by Temperature Swing Adsorption. *J. CO_2 Util.* **2017**, *21*, 261-269.

(14) Li, H.; Eddaoudi, M.; O'Keeffe, M.; Yaghi, O. M. Design and Synthesis of an Exceptionally Stable and Highly Porous Metal-Organic Framework. *Nature* **1999**, *402*, 276-279.

(15) Eddaoudi, M.; Kim, J.; Rosi, N.; Vodak, D.; Wachter, J.; O'Keeffe, M.; Yaghi, O. M. Systematic Design of Pore Size and Functionality in Isoreticular MOFs and their Application in Methane Storage. *Science* **2002**, *295*, 469-472.

(16) Chae, H. K.; Siberio-Pérez, D. Y.; Kim, J.; Go, Y.; Eddaoudi, M.; Matzger, A. J.; O'Keeffe, M.; Yaghi, O. M. A Route to High Surface Area, Porosity and Inclusion of Large Molecules in Crystals. *Nature* **2004**, *427*, 523-527.

(17) Ockwig, N. W.; Delgado-Friedrichs, O.; O'Keeffe, M.; Yaghi, O. M. Reticular Chemistry: Occurrence and Taxonomy of Nets and Grammar for the Design of Frameworks. *Accounts chem. Res.* **2005**, *38*, 176-182.

(18) Yaghi, O. M.; O'Keeffe, M.; Ockwig, N. W.; Chae, H. K.; Eddaoudi, M.; Kim, J. Reticular Synthesis and the Design of New Materials. *Nature* **2003**, *423*, 705-714.

(19) Kitagawa, S.; Kitaura, R.; Noro, S. I. Functional Porous Coordination Polymers. *Angew. Chem. Intl. Ed.* **2004**, *43*, 2334-2375.

(20) Kepert, C. J.; Prior, T. J.; Rosseinsky, M. J. A Versatile Family of Interconvertible Microporous Chiral Molecular Frameworks: the First Example of Ligand Control of Network Chirality. *J. Am. Chem. Soc.* **2000**, *122*, 5158-5168.

(21) Düren, T.; Sarkisov, L.; Yaghi, O. M.; Snurr, R. Q. Design of New Materials for Methane Storage. *Langmuir* **2004**, *20*, 2683-2689.

(22) Choi, S.; Drese, J. H.; Jones, C. W. Adsorbent Materials for Carbon Dioxide Capture from Large Anthropogenic Point Sources. *ChemSusChem* **2009**, *2*, 796-854.

(23) Wang, Q.; Luo, J.; Zhong, Z.; Borgna, A. CO_2 Capture by Solid Adsorbents and their Applications: Current Status and New Trends. *Energy Environ. Sci*. **2011**, *4*, 42-55.

(24) Liu, J.; Thallapally, P. K.; McGrail, B. P.; Brown, D. R.; Liu, J. Progress in Adsorption-Based CO_2 Capture by Metal-Organic Frameworks. *Chem. Soc. Rev*. **2012**, *41*, 2308-2322.

(25) Zhang, Z.; Yao, Z. Z.; Xiang, S.; Chen, B. Perspective of Microporous Metal-Organic Frameworks for CO_2 Capture and Separation. *Energy Environ. Sci*. **2014**, *7*, 2868-2899.

(26) Mason, J.A.; Sumida, K.; Herm, Z.R.; Krishna, R.; Long, J.R. Evaluating Metal-Organic Frameworks for Post-Combustion Carbon Dioxide Capture via Temperature Swing Adsorption. *Energy Environ. Sci*. **2011**, *4*, 3030-3040.

(27) Caskey, S. R.; Wong-Foy, A. G.; Matzger, A. J. Dramatic Tuning of Carbon Dioxide Uptake via Metal Substitution in a Coordination Polymer with Cylindrical Pores. *J. Am. Chem. Soc.* **2008**, *130*, 10870-10871.

(28) Dzubak, A. L.; Lin, L.-C.; Kim, J.; Swisher, J. A.; Poloni, R.; Maximoff, S. N.; Smit, B.; Gagliardi, L. Ab Initio Carbon Capture in Open-Site Metal Organic Frameworks. *Nat. Chem*. **2012**, *4*, 810–816.

(29) Ding, L.; Yazaydin, A. O. How Well do Metal–Organic Frameworks Tolerate Flue Gas Impurities?. *J. Phys. Chem. C* **2012**, *116*, 22987-22991.

(30) Fioretos, K. A.; Psofogiannakis, G. M.; Froudakis, G. E. Ab-Initio Study of the Adsorption and Separation of NOx and SOx Gases in Functionalized IRMOF Ligands. *J. Phys. Chem. C* **2011**, *115*, 24906-24914.

(31) Low, J. J.; Benin, A. I.; Jakubczak, P.; Abrahamian, J. F.; Faheem, S. A.; Willis, R. R. Virtual High Throughput Screening Confirmed Experimentally: Porous Coordination Polymer Hydration. *J. Am. Chem. Soc.* **2009**, *131*, 15834-15842.

(32) DeCoste, J. B.; Peterson, G. W.; Schindler, B. J.; Killops, K. L.; Browe, M. A.; Mahle, J. J. The Effect of Water Adsorption on the Structure of the Carboxylate Containing Metal–Organic Frameworks Cu-BTC, Mg-MOF-74, and UiO-66. *J. Mat. Chem. A* **2013**, *1*, 11922-11932.

(33) Glover, T. G.; Peterson, G. W.; Schindler, B. J.; Britt, D.; Yaghi, O. M. MOF-74 Building Unit has a Direct Impact on Toxic Gas Adsorption. *Chem. Eng. Sci.* **2011**, *66*, 163-170.

(34) Yu, J.; Ma, Y.; Balbuena, P. B. Evaluation of the Impact of H_2O, O_2, and SO_2 on Postcombustion CO_2 Capture in Metal–Organic Frameworks. *Langmuir* **2012**, *28*, 8064-8071.

(35) Sun, W.; Lin, L. C.; Peng, X.; Smit, B. Computational Screening of Porous Metal-Organic Frameworks and Zeolites for the Removal of SO_2 and NOx from Flue Gases. *AIChE J.* **2014**, *60*, 2314-2323.

(36) Liu, D.; Zhong, C. Understanding Gas Separation in Metal–Organic Frameworks using Computer Modeling. *J. Mater. Chem*. **2010**, *20*, 10308−10318

(37) Smit, B.; Maesen, T. L. M. Molecular Simulations of Zeolites: Adsorption, Diffusion, and Shape Selectivity. *Chem. Rev*. **2008**, *108*, 4125−4184.

(38) Cao, D.; Feng, P.; Wu, J. Molecular Simulation of Novel Carbonaceous Materials for Hydrogen Storage. *Nano Lett.* **2004**, *4*, 1489-1492.

(39) Krishna, R. Diffusion in porous crystalline materials. *Chem. Soc. Rev*. **2012**, *41*, 3099−3118

(40) Sillar, K.; Kundu, A.; Sauer, J. Ab Initio Adsorption Isotherms for Molecules with Lateral Interactions: CO_2 in Metal-Organic Frameworks. *J. Phys. Chem. C* **2017**, *121*, 12789-12799

(41) Kundu, A.; Piccini, G.; Sillar, K.; Sauer, J. Ab Initio Prediction of Adsorption Isotherms for Small Molecules in Metal−Organic Frameworks. *J. Am. Chem. Soc*. **2016**, *138*, 14047−14056.

(42) Kresse, G.; Furthmüller, J. Efficiency of Ab-Initio Total Energy Calculations for Metals and Semiconductiors Using Planewave Basis Set. *Comput. Mater. Sci.* **1996**, *6*, 15-50.

(43) Kresse, G.; Furthmüller, J. Efficient Iterative Schemes for Ab-Initio Total-Energy Calculations Using a Plane-Wave Basis Set. *Phys. Rev. B* **1996**, *54*, 11169-11186.

(44) Dion, M.; Rydberg, H.; Schröder, E.; Langreth, D.C.; Lundqvist, B.I. Van der Waals Density Functional for General Geometries. *Phys. Rev. Lett.* **2004**, *92*, 246401.

(45) Lee, K.; Murray, E.D.; Kong, L.; Lundqvist, B.I.; Langreth, D.C. Higher-Accuracy Van der Waals Density Functional. *Phys. Rev. B* **2010**, *82*, 081101.

(46) Vlaisavljevich, B.; Huck, J.; Hulvey, Z.; Lee, K.; Mason, J.A.; Neaton, J.B.; Long, J.R.; Brown, C.M.; Alfè, D.; Michaelides, A.; Smit, B. Performance of Van der Waals Corrected Functionals for Guest Adsorption in the M_2(dobdc) Metal-Organic Frameworks. *J. Phys. Chem A* **2017**, *121*, 4139-4151.

(47) Kresse, G.; Joubert, D. From Ultrasoft Pseudopotentials to the Projector Augmented-Wave Method. *Phys. Rev. B: Condens. Matter Mater. Phys*. **1999**, *59*, 1758-1775.

(48) McQuarrie, D.A. *Statistical Mechanics*; University Science Books: Sausalito, 2013

(49) Langmuir I. The Adsorption of Gases on Plane Surfaces of Glass, Mica and Platinum. *J. Am. Chem. Soc.* **1918**, *40*, 1361-1403.

(50) Sillar, K.; Sauer, J. Ab initio Prediction of Adsorption Isotherms for Small Molecules in Metal-Organic Frameworks: The effect of Lateral Interactios for Methane/CPO-27-Mg. *J. Am. Chem. Soc.* **2012**, *134*, 18354-18365

(51) Queen, W. L.; Hudson, M. R.; Bloch, E. D.; Mason, J. A.; Gonzalez, M. I.; Lee, J. S.; Gygi, D.; Howe, J. D.; Lee, K.; Darwish, T. A.; James, M. Comprehensive Study of Carbon Dioxide Adsorption in the Metal–Organic Frameworks M_2(dobdc) (M= Mg, Mn, Fe, Co, Ni, Cu, Zn). *Chem. Sci.* **2014**, *5*, 4569-4581.

(52) Yazaydin, A. O.; Snurr, R. Q.; Park, T. H.; Koh, K.; Liu, J.; LeVan, M. D.; Benin, A. I.; Jakubczak, P.; Lanuza, M.; Galloway, D. B.; Low, J. J. Screening of Metal−Organic Frameworks for Carbon Dioxide Capture from Flue Gas using a Combined Experimental and Modeling Approach. *J. Am. Chem. Soc*. **2009**, *131*, 18198–18199.

(53) Masel, I.D. *Principles of Adsorption and Reaction on Solid Surfaces*; John Wiley & Sons: New York, 1996.

(54) Becker, T.M.; Heinen, J.; Dubbeldam, D.; Lin, L.C.; Vlugt, T.J.H. Polarizable Force Fields for CO_2 and CH_4 Adsorption on Mg-Mof-74. *J. Phys. Chem. C* **2017**, *121*, 4659–4673.

(55) Milchev, A.; Paunov M. A Unified Model Description of Mobile and Localized Adsorption: I. MFA with Nonadditive Lateral Interactions - An Application to Disordered Adsorbed Monolayer on a Structureless Substrate. *Surf. Sci.* **1981**, *108*, 25-37.

(56) Milchev, A.; Binder, K. Monte Carlo Study of a Lattice Gas Model with Non-Additive Lateral Interactions. *Surf. Sci*. **1985**, *164*, 1-8.

(57) Somorjai, Y.L. *Introduction to Surface Chemistry and Catalysis*; John Wiley & Sons, Inc.: New Jersey, 2010.

(58) Sircar, S.; Mohr, R.; Ristic, C.; Rao, M.B. Isosteric Heat of Adsorption: Theory and Experiment. *J. Phys. Chem. B* **1999**, *103*, 6539-6546.

(59) Kenneth, W. *"Generalized Thermodynamic Relationships". Thermodynamics (5th ed)*; McGraw-Hill, Inc.: New York. 1988.

(60) Poloni, R.; Smit, B.; Neaton, J. B. CO_2 Capture by Metal–Organic Frameworks with van der Waals Density Functionals. *J. Phys. Chem. A,* **2012**, *116*, 4957−4964.

(61) Park J.; Kim, H.; Han, S. S.; Jung, Y. Tuning Metal−Organic Frameworks with Open-Metal Sites and Its Origin for Enhancing CO_2 Affinity by Metal Substitution. *J. Phys. Chem. Lett*. **2012**, *3*, 826−829.

(62) Lee, K.; Howe, J. D.; Lin, L.-C., Smit, B.; Neaton, J. B. Small-Molecule Adsorption in Open-Site Metal−Organic Frameworks: A Systematic Density Functional Theory Study for Rational Design. *Chem. Mater*. **2015**, *27*, 668−678.

(63) Yu, K.; Kiesling, K.; Schmidt, J R. Trace Flue Gas Contaminants Poison Coordinatively Unsaturated Metal–Organic Frameworks: Implications for CO_2 Adsorption and Separation. *J. Phys. Chem. C* **2012**, *116*, 20480-20488.

(64) Tan, K.; Zuluaga S.; Wang, H.; Canepa, P.; Soliman, K.; Cure, J.; Li, J.; Thonhauser, T.; Chabal, Y. J. Interaction of Acid Gases SO_2 and NO_2 with Coordinatively Unsaturated Metal Organic Frameworks: M-MOF-74 (M = Zn, Mg, Ni, Co). *Chem. Mater*. **2017**, *29*, 4227−4235.

(65) Wu, X.; Bao, Z.; Yuan, B.; Wang, J.; Sun, Y.; Luo, H; Deng, S. Microwave Synthesis and Characterization of MOF-74 (M = Ni, Mg) for Gas Separation. *Micropor. Mesopor. Mater*. **2013**, *180*, 114–122.

(66) Dietzel, P.D.; Besikiotis, V.; Blom, R. Application of Metal-Organic Frameworks with Coordinatively Unsaturated Metal Sites in Storage and Separation of Methane and Carbon Dioxide. *J. Mater. Chem*. **2009**, *19*, 7362-7370.

(67) D'alessandro, D.; Smit, B.; Long, J. R. Carbon Dioxide Capture: Prospects for New Materials. *Angew. Chem. Int. Ed*. **2010**, *49*, 6058− 6082.

(68) Granite, E. J.; Pennline, H. W.; Photochemical Removal of Mercury from Flue Gas. *Ind. Eng. Chem. Res*. **2002**, *41*, 5470-5476.

(69) Peng X, Cao D. Computational Screening of Porous Carbons, Zeolites, and Metal Organic Frameworks for Desulfurization and Decarburization of Biogas, Natural Gas, and Flue Gas. *AIChE J.* **2013**, *59,* 2928–2942.

(70) Bloch, E.D.; Murray, L.J.; Queen, W.L.; Chavan, S.; Maximoff, S.N.; Bigi, J.P.; Krishna, R.; Peterson, V.K.; Grandjean, F.; Long, G.J.; Smit, B.; Bordiga, S.; Brown, C.M.; Long, J.R. Selective Binding of O_2 over N_2 in a Redox-Active Metal-Organic Framework with Open Iron(II) Coordination Sites. *J. Am. Chem. Soc*. **2011**, 113, 14814-14822.

(71) Ribeiro, R.; Grande, C. A.; Rodrigues, A. E. Electric swing adsorption for gas separation and purification: a review. *Sep. Sci. Technol*. **2014**, *49*, 1985-2002.

(72) Sircar, S. Basic research needs for design of adsorptive gas separation processes. *Ind. Eng. Chem. Res*. **2006**, *45*, 5435-5448.

(73) Granato, M. A.; Vlugt, T. J. H.; Rodrigues, A. E. Molecular simulation of propane-propylene binary adsorption equilibrium in zeolite 13X. *Ind. Eng. Chem. Res*. **2007**, *46*, 7239-7245.

(74) Ishibashi, M.; Ota, H.; Akutsu, N.; Umeda, S.; Tajika, M.; Izumi, J.; Yasutake, A.; Kabata, T.; Kageyama, Y. Technology for removing carbon dioxide from power plant flue gas by the physical adsorption method. *Energy Convers. Manage*. **1996**, *37*, 929–933.

(75) Wiersum, D.; Chang, J. S.; Serre, C.; Llewellyn, P. L. An adsorbent performance indicator as a first step evaluation of novel sorbents for gas separations: application to metal-organic frameworks. *Langmuir* **2013**, *29*, 3301-3309.